Chinese Journal of Aeronautics, (2013),26(6): 1471–1476

Chinese Society of Aeronautics and Astronautics
& Beihang University

Chinese Journal of Aeronautics

cja@buaa.edu.cn
www.sciencedirect.com

# Source localization using a non-cocentered orthogonal loop and dipole (NCOLD) array

**Liu Zhaoting** [a,*], **Xu Tongyang** [b]

[a] *Department of Electrical Engineering, Shaoxing University, Shaoxing 312000, China*
[b] *School of Information Management, Shanxi University of Finance and Economics, Taiyuan 030006, China*

Received 5 September 2012; revised 7 January 2013; accepted 9 July 2013
Available online 6 November 2013

**KEYWORDS**

Array signal processing;
Direction of arrival (DOA) estimation;
Electromagnetic vector-sensor array;
Polarization;
Source localization

**Abstract** A uniform array of scalar-sensors with intersensor spacings over a large aperture size generally offers enhanced resolution and source localization accuracy, but it may also lead to cyclic ambiguity. By exploiting the polarization information of impinging waves, an electromagnetic vector-sensor array outperforms the unpolarized scalar-sensor array in resolving this cyclic ambiguity. However, the electromagnetic vector-sensor array usually consists of cocentered orthogonal loops and dipoles (COLD), which is easily subjected to mutual coupling across these cocentered dipoles/loops. As a result, the source localization performance of the COLD array may substantially degrade rather than being improved. This paper proposes a new source localization method with a non-cocentered orthogonal loop and dipole (NCOLD) array. The NCOLD array contains only one dipole or loop on each array grid, and the intersensor spacings are larger than a half-wavelength. Therefore, unlike the COLD array, these well separated dipoles/loops minimize the mutual coupling effects and extend the spatial aperture as well. With the NCOLD array, the proposed method can efficiently exploit the polarization information to offer high localization precision.



## 1. Introduction

Source localization using a sensor array is fundamental in radar, sonar, navigation, geophysics, and acoustic tracking. The electromagnetic vector sensor array, with the available polarization information of impinging wave-fields, can offer better localization performance than the unpolarized scalar sensor array. Hence, it has attracted increasing interest for subspace-based direction of arrival (DOA) and polarization estimation, and based on this many array signal processing techniques have been developed (see Refs. [1–11]).

However, an electromagnetic vector-sensor is usually configured by 2 to 6 cocentered orthogonal loops and dipoles (COLD). Hence, in practical applications, the electromagnetic vector-sensor array, i.e., the COLD array, is easily subjected to mutual coupling across these collocated dipoles and loops.[1,2] With no effective electromagnetic isolation among them, the source localization performance of the COLD array will substantially degrade. Therefore, it is of practical importance to investigate the use of polarization information to improve the localization performance with no mutual coupling effects.

* Corresponding author. Tel.: +86 575 88341661.
E-mail address: liuzhaoting@163.com (Z. Liu).

Peer review under responsibility of Editorial Committee of CJA.

Production and hosting by Elsevier


http://dx.doi.org/10.1016/j.cja.2013.10.010

It is well known that a large array aperture in a sensor array generally offers enhanced array resolution and localization accuracy. But adding array elements to extend array length would increase hardware costs and the computational load required by the signal processors; hence it may be more advisable to obtain a large array aperture by using a sparse array.[4,5,12–14] The sparse array could also alleviate the mutual coupling effects among sensors on the sparse array-grids. However, non-uniform intersensor spacing over a large aperture necessitates the use of a computationally expensive iterative method of multiple signal classification (MUSIC) for DOA estimation. Whereas extending the uniform intersensor spacing beyond a half-wavelength will incur a set of cyclically ambiguous DOA estimates in accordance with the spatial Nyquist sampling theorem, and this cyclic ambiguity cannot be resolved without a priori source information using the customary unpolarized scalar-sensor array. To resolve cyclic ambiguity, Zoltowski and Wong creatively combined the vector cross-product approach with the estimation of signal parameters via rotational invariance technique (ESPRIT) to develop an extended aperture DOA estimator[4,5] with a sparse uniform electromagnetic vector-sensor array. Although the estimator is very efficient, the adopted vector-sensor model has not accounted for mutual coupling across the vector-sensor's COLD.

In this paper, we consider a uniform rectangular array with non-cocentered orthogonal loops and dipoles (NCOLD) for source localization. The NCOLD array contains only one dipole or loop on every uniform array-grid, and the intersensor spacings are allowed larger than a half-wavelength. Therefore, unlike the existing COLD array, these non-cocentered and well-separated dipole-loop sensors minimize mutual coupling effects while extending the spatial aperture. With the NCOLD array, we propose a new extended aperture DOA estimator, and show that the polarization information can still be fully exploited for enhanced array resolution and localization precision. Moreover, with a pre-processing procedure, the proposed algorithm can be extended to estimate DOAs in a multipath environment. Although the electromagnetic vector-sensor array enables one to decorrelate the coherency of incident signals by polarization smoothing (PS),[7] this smoothing processing makes it impossible for the polarization information to be further utilized for resolving the aforementioned cyclic ambiguity. Hence, the PS-based DOA algorithm also requires the inter-vector-sensor spacing within a half-wavelength, like the spatial smoothing (SS)-based DOA algorithm[15] with an unpolarized scalar-sensor array.

## 2. Problem formulation and modeling

Assume that $K$ uncorrelated transverse electromagnetic plane waves impinge upon a uniform rectangular array (URA) with a total of $6L$ ($K < 6L$) NCOLD. Unlike the COLD array, the NCOLD array contains only one dipole or loop at every array-grid $(i\Delta_x, \ell\Delta_y)$ for $\{i = 1,2,\ldots,6;\ \ell = 1,2,\ldots,L\}$, where $\Delta_x$ and $\Delta_y$ are respectively inter-sensor spacings along the $x$-axis and $y$-axis, and are far beyond the half-wavelength. We here refer the dipole parallel to the $x$-axis as the $x$-dipole and the loop parallel to the $x$-plane as the $x$-loop; the same is true for the $y$-dipole, $y$-loop, $z$-dipole and $z$-loop. Moreover, we let the NCOLD array's 1st, 2nd and 3rd rows contain $L$ $y$-dipoles, $z$-dipoles and $x$-dipoles, respectively, while the 4th, 5th and 6th rows contain $L$ $x$-loops, $z$-loops and $y$-loops, respectively, as shown in Fig. 1.

Without loss of generality, we let the array-grid (0, 0) be a reference. For each column of the array, there are three dipoles and three loops, all orthogonally oriented but with distinct phase centers, and these displaced dipoles/loops can produce a steering vector as

$$\tilde{\boldsymbol{c}}_k \overset{\text{def}}{=} \begin{bmatrix} \tilde{c}_{1,k} \\ \tilde{c}_{2,k} \\ \tilde{c}_{3,k} \\ \tilde{c}_{4,k} \\ \tilde{c}_{5,k} \\ \tilde{c}_{6,k} \end{bmatrix} \overset{\text{def}}{=} \begin{bmatrix} e_{y,k} \\ e_{z,k}q_{x,k} \\ e_{x,k}q_{x,k}^2 \\ h_{x,k}q_{x,k}^3 \\ h_{z,k}q_{x,k}^4 \\ h_{y,k}q_{x,k}^5 \end{bmatrix} = \boldsymbol{c}_k \odot \boldsymbol{q}_{x,k} \tag{1}$$

where $\odot$ denotes the element-wise multiplication between two vectors, $\boldsymbol{q}_{x,k} = [\mathbf{1} q_{x,k} \cdots q_{x,k}^5]^{\mathrm{T}}$ with $\boldsymbol{q}_{x,k} = \mathrm{e}^{\mathrm{j}2\pi u_k \Delta_x/\lambda}$ and $\boldsymbol{u}_k = \sin\theta_k\cos\phi_k$ symbolizing respectively the spatial phase factor and the direction-cosine along the $x$-axis, $\lambda$ denotes the signal wave length, $\boldsymbol{c}_k$ is equal to a steering vector of the typical six-component electromagnetic vector-sensor and can be expressed by

$$\boldsymbol{c}_k = \begin{bmatrix} \sin\varphi_k\cos\theta_k & \cos\varphi_k \\ \sin\theta_k & 0 \\ \cos\varphi_k\cos\theta_k & -\sin\varphi_k \\ -\sin\varphi_k & -\cos\varphi_k\cos\theta_k \\ 0 & \sin\theta_k \\ \cos\varphi_k & -\sin\varphi_k\cos\theta_k \end{bmatrix} \begin{bmatrix} \sin\gamma_k \mathrm{e}^{\mathrm{j}\eta_k} \\ \cos\gamma_k \end{bmatrix} \triangleq \begin{bmatrix} e_{y,k} \\ e_{z,k} \\ e_{x,k} \\ h_{x,k} \\ h_{z,k} \\ h_{y,k} \end{bmatrix} \tag{2}$$

where $\theta_k \in [0, \pi/2)$ denotes the $k$th incident source's elevation-angle measured from the positive $z$-axis, $\varphi_k \in [0, 2\pi)$ signifies the azimuth-angle measured from the positive $x$-axis, $\gamma_k \in [0, \pi/2)$ refers to the auxiliary polarization angle, and $\eta_k \in [\pi, \pi)$ represents the polarization phase difference. The $6L \times 1$ array manifold $\boldsymbol{a}(\theta_k, \varphi_k, \gamma_k, \eta_k) = \boldsymbol{a}_k$ for the entire $6L$-element array is

$$\boldsymbol{a}_k = \tilde{\boldsymbol{c}}_k \otimes \underbrace{\begin{bmatrix} 1 \\ q_{y,k} \\ \vdots \\ q_{y,k}^{L-1} \end{bmatrix}}_{\boldsymbol{q}_{y,k}} = \begin{bmatrix} \tilde{c}_{1,k}\boldsymbol{q}_{y,k} \\ \tilde{c}_{2,k}\boldsymbol{q}_{y,k} \\ \tilde{c}_{3,k}\boldsymbol{q}_{y,k} \\ \tilde{c}_{4,k}\boldsymbol{q}_{y,k} \\ \tilde{c}_{5,k}\boldsymbol{q}_{y,k} \\ \tilde{c}_{6,k}\boldsymbol{q}_{y,k} \end{bmatrix} = (\boldsymbol{c}_k \odot \boldsymbol{q}_{x,k}) \otimes \boldsymbol{q}_{y,k} \tag{3}$$

where $\boldsymbol{q}_{y,k} = \mathrm{e}^{\mathrm{j}2\pi v_k \Delta_y/\lambda}$ and $v_k = \sin\theta_k \sin\varphi_k$ symbolize respectively the spatial phase factor and the direction-cosine along

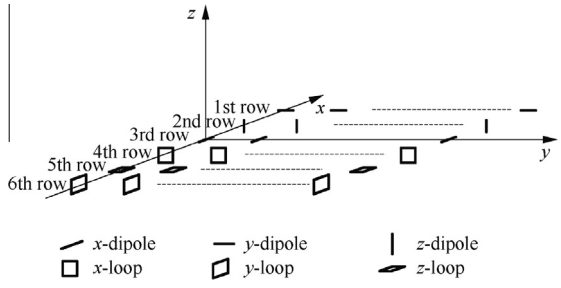


**Fig. 1** The proposed NCOLD array.

the $y$-axis. With a total of $K$ signal sources, the entire array would yield a vector measurement

$$\boldsymbol{z}(t) = [\boldsymbol{z}_1\, \boldsymbol{z}_2 \cdots \boldsymbol{z}_L]^{\mathrm{T}} = \sum_{k=1}^{K} \boldsymbol{a}_k s_k(t) + \boldsymbol{n}(t) \tag{4}$$

where $\boldsymbol{z}_\ell = [z_{1,\ell}\, z_{2,\ell} \cdots z_{6,\ell}]$, $z_{i,\ell}$ is the received signal of the $(i,\ell)$th sensor located at the array-grid $(i\Delta_x,\ \ell\Delta_y)$, $\boldsymbol{A} = [\boldsymbol{a}_1\, \boldsymbol{a}_2 \cdots \boldsymbol{a}_K]^{\mathrm{T}}$, $\boldsymbol{s}_k(t) = [s_1(t)\, s_2(t) \cdots s_k(t)]^{\mathrm{T}}$, $s_k(t)$ symbolizes the $k$th source's complex envelope, and $\boldsymbol{n}(t)$ is an additive spatio-temporally uncorrelated Gaussian noise vector with a zero mean. The objective of the source localization is to determine the two-dimensional (2D) DOAs $\{\theta_k,\ \varphi_k,\ k = 1, 2, \cdots, K\}$.

## 3. Estimating the 2D DOAs using the presented array

In this section, we use the presented array to estimate the 2D DOAs, and improve the estimation performance by increasing $\Delta_x$ and $\Delta_y$.

### 3.1. Deriving coarse direction cosine estimates

We first divide the $6L \times 1$ matrix $\boldsymbol{A}$ into six parts as follows:

$$\boldsymbol{A} = [\boldsymbol{A}_1^{\mathrm{H}}\ \boldsymbol{A}_2^{\mathrm{H}} \cdots \boldsymbol{A}_6^{\mathrm{H}}]^{\mathrm{H}} \tag{5}$$

where $\boldsymbol{A}_i = [\tilde{c}_{i,1}\boldsymbol{q}_{y,1}\ \tilde{c}_{i,2}\boldsymbol{q}_{y,2} \cdots \tilde{c}_{i,K}\boldsymbol{q}_{y,K}] \in \mathbf{C}^{L\times K}$ $(i = 1,\ 2, \cdots, 6)$ are sub-matrices, and they are related to each other by

$$\boldsymbol{A}_i = \boldsymbol{A}_1 \boldsymbol{\Lambda}_i \tag{6}$$

with $\boldsymbol{\Lambda}_i = \mathrm{diag}(d_{i,1},\ d_{i,2}, \cdots, d_{i,K})$, $d_{i,k} = \tilde{c}_{i,k}/\tilde{c}_{1,k}$ $(k = 1, 2, \cdots, K)$. Using the subspace techniques, we perform eigen-decomposition on the following array covariance matrix

$$\boldsymbol{R} = E[\boldsymbol{z}(t)\boldsymbol{z}^{\mathrm{H}}(t)] = \boldsymbol{A}\boldsymbol{S}\boldsymbol{A}^{\mathrm{H}} + \sigma^2\boldsymbol{I}_{6L} \tag{7}$$

where $\boldsymbol{S} = E[\boldsymbol{s}(t)\boldsymbol{s}^{\mathrm{H}}(\boldsymbol{t})]$ is the source covariance matrix; we then obtain a signal subspace matrix $\boldsymbol{U} \in \mathrm{C}^{6L\times 1}$, which is composed of the $K$ eigenvectors corresponding to the largest $K$ eigenvalues of $\boldsymbol{R}$. The matrix $\boldsymbol{U}$ is related to $\boldsymbol{A}$ by a unique nonsingular matrix $\boldsymbol{T}$ as

$$\boldsymbol{U} = \boldsymbol{A}\boldsymbol{T} = \begin{bmatrix} \boldsymbol{A}_1\boldsymbol{T} \\ \boldsymbol{A}_2\boldsymbol{T} \\ \vdots \\ \boldsymbol{A}_6\boldsymbol{T} \end{bmatrix} = \begin{bmatrix} \boldsymbol{U}_1 \\ \boldsymbol{U}_2 \\ \vdots \\ \boldsymbol{U}_6 \end{bmatrix} \tag{8}$$

with $\boldsymbol{U}_i = \boldsymbol{A}_i\boldsymbol{T}$. From Eqs. (6) and (8), we have

$$\boldsymbol{U}_1^{\dagger}\boldsymbol{U}_i = \boldsymbol{T}^{-1}\boldsymbol{\Lambda}_i\boldsymbol{T} \tag{9}$$

This implies that the diagonal elements $d_{i,k}$ $(k = 1, 2, \cdots, K;\ i = 2, 3, \cdots, 6)$ of the matrix $\boldsymbol{\Lambda}_i$ can be obtained by finding the eigenvalues of $\boldsymbol{U}_1^{\dagger}\boldsymbol{U}_i$.

Let

$$\begin{cases} \widetilde{\boldsymbol{E}}_k = \begin{bmatrix} d_{3,k} \\ 1 \\ d_{2,k} \end{bmatrix} \\ \widetilde{\boldsymbol{H}}_k = \begin{bmatrix} d_{4,k} \\ d_{6,k} \\ d_{5,k} \end{bmatrix} \end{cases} \tag{10}$$

It is easy to prove that the Frobenius norm of either $\widetilde{\boldsymbol{E}}_k$ and $\widetilde{\boldsymbol{H}}_k$ equals one. Performing cross-product of the vectors $\widetilde{\boldsymbol{E}}_k$ and $\widetilde{\boldsymbol{H}}_k$ yields

$$\frac{\widetilde{\boldsymbol{E}}_k \times \widetilde{\boldsymbol{H}}_k^*}{\|\widetilde{\boldsymbol{E}}_k \times \widetilde{\boldsymbol{H}}_k^*\|} = \frac{\boldsymbol{E}_k \times \boldsymbol{H}_k^*}{\|\boldsymbol{E}_k \times \boldsymbol{H}_k^*\|} \odot \begin{bmatrix} q_{x,k}^{-4} \\ q_{x,k}^{-2} \\ q_{x,k}^{-3} \end{bmatrix} = \begin{bmatrix} u_k q_{x,k}^{-4} \\ v_k q_{x,k}^{-2} \\ w_k q_{x,k}^{-3} \end{bmatrix} \stackrel{\mathrm{def}}{=} \boldsymbol{\zeta}_k \tag{11}$$

where $^*$ denotes complex conjugation, $\boldsymbol{E}_k = [e_{x,k}\, e_{y,k}\, e_{z,k}]^{\mathrm{T}}$ and $\boldsymbol{H}_k = [h_{x,k}\, h_{y,k}\, h_{z,k}]^{\mathrm{T}}$ respectively are the electric-field and magnetic-field vectors of the impinging electromagnetic waves, and $w_k = \cos\theta_k$ signifies the spatial phase factor along the $z$-axis.

In realistic cases where noise is present and only finite snapshots are available, the array covariance matrix $\boldsymbol{R}$ in Eq. (7) is obtained by using the following estimation

$$\widehat{\boldsymbol{R}} = \sum_{n=1}^{N} \boldsymbol{z}(\boldsymbol{t}_n)\boldsymbol{z}^{\mathrm{H}}(t_n)/N \tag{12}$$

where $N$ is the snapshot number. Therefore, the relationship in Eq. (11) becomes only approximate. In addition, since the independent eigen-decompositions of $\boldsymbol{U}_1^{\dagger}\boldsymbol{U}_i$ $(i = 2,\ 3, \cdots, 6)$ lead to an arbitrary ordering of the diagonal elements in $\boldsymbol{\Lambda}_i$, we need to pair the elements of the five sets of parameters $\{d_{i,1}, d_{i,2}, \cdots, d_{i,K}\}$ for the DOA estimation. Fortunately, $\boldsymbol{U}_1^{\dagger}\boldsymbol{U}_i$ have the same sets of eigenvectors, so the eigenvalues can be paired in a manner similar to that of,[10] by matching the eigenvectors of $\boldsymbol{U}_1^{\dagger}\boldsymbol{U}_i$.

Subsequently, we use the relationship in Eq. (11) to compute direction-cosine estimates. Note that $\{u_k,\ v_k,\ w_k\}$ are "modulated" by the $x$-axis spatial phase factor $q_{x,k}$ in Eq. (11), but their absolute-values can be estimated as $|\zeta_k(1)| = |\hat{u}_k\hat{q}_{x,k}^{-4}| = |\hat{u}_k|$, $|\zeta_k(2)| = |\hat{v}_k\hat{q}_{x,k}^{-2}| = |\hat{v}_k|$ and $|\zeta_k(3)| = |\hat{w}_k\hat{q}_{x,k}^{-3}| = |\hat{w}_k|$, respectively. Due to the assumption of $\theta_k \in [0, \pi/2)$ and $\varphi_k \in [0, 2\pi)$, the estimation of $w_k$ can be directly given as

$$\hat{w}_k = |\zeta_k(3)| \tag{13}$$

where as a further determination is needed for the estimation of $u_k$ and $v_k$. For this purpose, we let

$$\tau_{uw} = \frac{\zeta_k^3(1)}{\zeta_k^4(3)} = \frac{\hat{u}_k^3\hat{q}_{x,k}^{-12}}{\hat{w}_k^4\hat{q}_{x,k}^{-12}} = \frac{\hat{u}_k^3}{\hat{w}_k^4} \tag{14}$$

It is clear that, if $\tau_{uw} > 0$, then $\hat{u}_k > 0$, otherwise $\hat{u}_k \leqslant 0$. Therefore, we can determine the estimation of $u_k$ as

$$\hat{\boldsymbol{u}}_k = \begin{cases} |\zeta_k(1)|, & \tau_{uw} > 0 \\ -|\zeta_k(1)|, & \tau_{uw} \leqslant 0 \end{cases} \tag{15}$$

In a similar way, with $\tau_{vw} = \dfrac{\zeta_k^3(1)}{\zeta_k^2(3)}$, the estimation of $v_k$ can be given as

$$\hat{v}_k = \begin{cases} |\zeta_k(2)|, & \tau_{vw} > 0 \\ -|\zeta_k(2)|, & \tau_{vw} \leqslant 0 \end{cases} \tag{16}$$

Intuitively, the estimates $\{\hat{u}_k, \hat{v}_k, \hat{w}_k\}$ are extracted from the electric-field and magnetic-field vectors of a vector sensor which has no effective geometric aperture. Hence, they are unambiguous regardless of the sizes of the inter-sensor spacings $\Delta_x$ and $\Delta_y$, but may be coarse. A refined vision of direction-cosine estimates can be obtained by using the spatial phase factor $\boldsymbol{q}_{x,k}$ and $\boldsymbol{q}_{y,k}$, which are related to the array's geometric aperture.

### 3.2. Deriving the refined x-axis direction cosine estimates

From Eq. (11), the estimates $\{\hat{u}_k, \hat{v}_k, \hat{w}_k\}$ can further lead to the estimation of the $x$-axis spatial phase factor $q_{x,k}$:

$$\hat{q}_{x,k} = \frac{1}{2}\left(\frac{\hat{\zeta}_k(1)\hat{w}_k}{\hat{\zeta}_k(3)\hat{u}_k} + \frac{\hat{\zeta}_k(3)\hat{v}_k}{\hat{\zeta}_k(2)\hat{w}_k}\right) \quad (k = 1,\ 2, \cdots, K) \tag{17}$$

Thus, the estimation of direction cosine $u_k$ can also be easily extracted from $\hat{q}_{x,k}$. According to the uniform sparse array-spacing principle,[4,5] we have a set of cyclically related candidates for the estimation of $u_k$

$$\hat{u}_k(n_{u,k}) = \mu_k + n_{u,k}\lambda/\Delta_x \tag{18}$$

where $\mu_k = \frac{\lambda}{2\pi\Delta_x}\arg\{\hat{q}_{x,k}\}$, $n_u$ is an integer and $\text{ceil}\{-\Delta_x(1+\mu_k)/\lambda\} \leqslant n_u \leqslant \text{floor}\{\Delta_x(1-\mu_k)/\lambda\}$, $\text{floor}\{x\}$ indicates the largest integer not greater than $x$, and $\text{ceil}\{x\}$ indicates the smallest integer not less than $x$.

To resolve the cyclic ambiguity in Eq. (18), we let $\hat{u}_k$ in Eq. (15) be coarse references, and then the refined direction cosine estimates can be given as

$$\hat{u}_k^{\text{refined}} = \mu_k + n_{u,k}^0\lambda/\Delta_x \tag{19}$$

where $n_{u,k}^0 = \underset{n_{u,k}}{\text{argmin}}\,|\hat{u}_k(n_{u,k}) - \hat{u}_k|$.

### 3.3. Deriving the refined y-axis direction cosine estimates

To derive the refined $y$-axis direction-cosine estimates $\hat{v}_k^{\text{refined}}$, we use Eq. (8) to define sub-matrices

$$\boldsymbol{U}^{\text{f}} = \begin{bmatrix}\boldsymbol{U}_1^{\text{f}}\\ \boldsymbol{U}_2^{\text{f}}\\ \vdots\\ \boldsymbol{U}_6^{\text{f}}\end{bmatrix} = \begin{bmatrix}\boldsymbol{A}_1^{\text{f}}\\ \boldsymbol{A}_2^{\text{f}}\\ \vdots\\ \boldsymbol{A}_6^{\text{f}}\end{bmatrix}\boldsymbol{T} \quad \text{and} \quad \boldsymbol{U}^{\text{b}} = \begin{bmatrix}\boldsymbol{U}_1^{\text{b}}\\ \boldsymbol{U}_2^{\text{b}}\\ \vdots\\ \boldsymbol{U}_6^{\text{b}}\end{bmatrix} = \begin{bmatrix}\boldsymbol{A}_1^{\text{b}}\\ \boldsymbol{A}_2^{\text{b}}\\ \vdots\\ \boldsymbol{A}_6^{\text{b}}\end{bmatrix}\boldsymbol{T}$$

where $\boldsymbol{U}_i^{\text{f}}$ and $\boldsymbol{A}_i^{\text{f}}$ ($i = 1, 2, \cdots, 6$) are respectively the first $L-1$ rows of $\boldsymbol{U}_i$ and $\boldsymbol{A}_i$, while $\boldsymbol{U}_i^{\text{b}}$ and $\boldsymbol{A}_i^{\text{b}}$ are respectively the last $L-1$ rows of $\boldsymbol{U}_i$ and $\boldsymbol{A}_i$. It can be proven that

$$\boldsymbol{U}^{\text{b}}\boldsymbol{T}^{-1}\boldsymbol{\Upsilon}\boldsymbol{T} = \boldsymbol{A}^{\text{b}}\boldsymbol{\Upsilon}\boldsymbol{T} = \boldsymbol{A}^{\text{f}}\boldsymbol{T} = \boldsymbol{U}^{\text{f}} \tag{20}$$

where $\boldsymbol{\Upsilon} = \text{diag}(q_{y,1},\ q_{y,2}, \cdots, q_{y,K})$.

Eq. (20) shows the $y$-axis spatial phase factor estimates $\{\hat{q}_{y,1},\ \hat{q}_{y,2}, \cdots, \hat{q}_{y,K}\}$ can also be obtained from $K$ eigenvalues of matrix $(\boldsymbol{U}^{\text{b}})^{\dagger}\boldsymbol{U}^{\text{f}}$. Therefore, using the same way as exploited in the derivation of $\hat{u}_k$, we obtain

$$\hat{v}_k^{\text{refined}} = \upsilon_k + n_{v,k}^0\lambda/\Delta_y \tag{21}$$

where $\text{ceil}\{-\Delta_y(1+\mu_k)/\lambda\} \leqslant n_v \leqslant \text{floor}\{\Delta_y(1-\mu_k)/\lambda\}$, $\upsilon_k = \frac{\lambda}{2\pi\Delta_y}\arg\{\hat{q}_{y,k}\}$, $n_{v,k}^0 = \underset{n_{v,k}}{\text{argmin}}\,|\hat{v}_k(n_{v,k}) - \hat{v}_k|$, and $\hat{v}_k(n_{v,k}) = \mu_k + n_{v,k}\lambda/\Delta_y$. From the foregoing analysis, the 2D DOAs can be estimated as $\hat{\theta}_k = \arcsin\left(\sqrt{(\hat{u}_k^{\text{refined}})^2 + (\hat{v}_k^{\text{refined}})^2}\right)$ and $\hat{\varphi}_k = \angle\left(\hat{u}_k^{\text{refined}} + \text{j}\hat{v}_k^{\text{refined}}\right)$.

## 4. DOA estimation in a multipath environment

In multipath propagation environments, there are often highly correlated or coherent sources. Since the coherent signals will cause rank deficiency of the noiseless correlation matrix, a pre-processing procedure is needed to decorrelate the coherency of incident signals.

We define a cross-correlation between $(n, m)$th sensor and $(i, \ell)$th sensor as

$$r_{n,m}^{i,\ell} = E[z_{n,m}z_{i,\ell}^*] = \sum_{k=1}^{K}\tilde{c}_n q_{y,k}^{m-1}E[s_k s_k^*]\tilde{c}_i^*(q_{y,k}^{\ell-1})^* \tag{22}$$

Then, two Hankel matrices are constructed from $r_{n,m}^{i,\ell}$ with $m = 1, 2, \cdots, L$ as follows

$$\begin{cases}\boldsymbol{R}^{\text{f}}(n;i) = \begin{bmatrix} r_{n,1}^{i,L} & r_{n,2}^{i,L} & \cdots & r_{n,K}^{i,L}\\ r_{n,2}^{i,L} & r_{n,3}^{i,L} & \cdots & r_{n,K+1}^{i,L}\\ \vdots & \vdots & & \vdots\\ r_{n,M}^{i,L} & r_{n,M+1}^{i,L} & \cdots & r_{n,L-1}^{i,L}\end{bmatrix}\\ \boldsymbol{R}^{\text{b}}(n;i) = \begin{bmatrix} r_{n,2}^{i,1} & r_{n,3}^{i,1} & \cdots & r_{n,K+1}^{i,1}\\ r_{n,3}^{i,1} & r_{n,4}^{i,1} & \cdots & r_{n,K+2}^{i,1}\\ \vdots & \vdots & & \vdots\\ r_{n,M+1}^{i,1} & r_{n,M+2}^{i,1} & \cdots & r_{n,L}^{i,1}\end{bmatrix}\end{cases}$$

where $M = L - K > K$. We can easily prove that the two $\boldsymbol{R}^{\text{f}}(n;i)$ and $\boldsymbol{R}^{\text{b}}(n;i)$ are of full rank. Further, let

$$\begin{cases}\boldsymbol{R}^{\text{f}} = \begin{bmatrix}\boldsymbol{R}^{\text{f}}(1;1) & \boldsymbol{R}^{\text{f}}(1;2) & \cdots & \boldsymbol{R}^{\text{f}}(1;6)\\ \boldsymbol{R}^{\text{f}}(2;1) & \boldsymbol{R}^{\text{f}}(2;2) & \cdots & \boldsymbol{R}^{\text{f}}(2;6)\\ \vdots & \vdots & & \vdots\\ \boldsymbol{R}^{\text{f}}(6;1) & \boldsymbol{R}^{\text{f}}(6;2) & \cdots & \boldsymbol{R}^{\text{f}}(6;6)\end{bmatrix}\\ \boldsymbol{R}^{\text{b}} = \begin{bmatrix}\boldsymbol{R}^{\text{b}}(1;1) & \boldsymbol{R}^{\text{b}}(1;2) & \cdots & \boldsymbol{R}^{\text{b}}(1;6)\\ \boldsymbol{R}^{\text{b}}(2;1) & \boldsymbol{R}^{\text{b}}(2;2) & \cdots & \boldsymbol{R}^{\text{b}}(2;6)\\ \vdots & \vdots & & \vdots\\ \boldsymbol{R}^{\text{b}}(6;1) & \boldsymbol{R}^{\text{b}}(6;2) & \cdots & \boldsymbol{R}^{\text{b}}(6;6)\end{bmatrix}\end{cases}$$

and finally, the following matrix

$$\widetilde{\boldsymbol{R}} = \boldsymbol{R}^{\text{f}} + \boldsymbol{R}^{\text{b}} \tag{23}$$

can displace the matrix $\boldsymbol{R}$ in Eq. (7) to derive DOA estimates in similar steps.

For a sparse array, the sensors are sparsely placed so that the noise at each sensor is essentially uncorrelated. However, the noise power of each sensor can still be different due to the nonuniformity of sensor noise. Owing to the use of cross-correlation matrices between different sensors, the proposed algorithm for coherent signals' DOA estimation can be extended to such nonuniform white noise. Therefore, the proposed algorithm has two notable advantages over the polarization smoothing (PS)-based[7] or the popular spatial smoothing (SS)-based[15] estimation algorithms: less restrictive intersensor spacing and less restrictive noise model.

## 5. Simulation results

Computer simulations are carried out to illustrate the performance of the proposed algorithm with a $6 \times 6$ NCOLD containing a total of 36 dipoles/loops (i.e., $L = 6$). The performance metric used is the root mean squared error (RMSE), defined as $\text{RMSE}_k = \sqrt{E\{(\hat{\theta}_k - \theta_k)^2 + (\hat{\varphi}_k - \varphi_k)^2\}}$[16–20] and each data point in each

figure given below is averaged over 500 independent Monte-Carlo trials. Two equal-power narrowband signals impinge on the arrays with the following DOA and polarization parameters: $\theta_1 = 65°$, $\varphi_1 = 45°$, $\gamma_1 = 45°$, $\eta_1 = 90°$, $\theta_2 = 70°$, $\varphi_2 = 40°$, $\gamma_2 = 45°$, $\eta_2 = 90°$. Besides, the snapshot number is $N = 100$ with no special emphasis.

In the first example, assuming the two signals are uncorrelated, we examine the performance of the proposed algorithm with respect to the intersensor spacing $\Delta_x = \Delta_y = \Delta$, by comparing to the extended-aperture (EA) algorithm[4] with a COLD array and the unitary ESPRIT (U-ESPRIT) algorithm[16] with an unpolarized scalar-sensor (USS) array. For comparison purposes, the USS array consists of 36 unpolarized scalar-sensors forming a $6 \times 6$ uniform rectangular geometry, and the COLD array contains 9 six-component electromagnetic vector-sensors constituting a $3 \times 3$ uniform rectangular geometry. Since the U-ESPRIT algorithm, when ignoring the polarization information, is only applicable to a case of the intersensor spacing within $\lambda/2$, we herein keep its intersensor spacing $\Delta = \lambda/2$.

The result for the first signal source is shown in Fig. 2. It is observed that the performance of the proposed algorithm is close to the Cramer–Rao lower bound (CRLB), except at the rather too large intersensor spacing $\Delta$. The RMSEs of the proposed algorithm and the EA algorithm decrease linearly with the increase of intersensor spacing $\Delta$, and are much lower than those of the U-ESPRIT algorithm. When further increasing the intersensor spacing to $\Delta > 32\lambda$ for the proposed algorithm, the RMSEs of the refined estimates begin to increase and are close to those of the coarse estimates. The same phenomenon occurs for the EA algorithm when $\Delta > 14\lambda$. This is due to the fact[4,5] that increasing $\Delta$ causes a gradual approach of the ambiguous solution set and the coarse references, and hence it becomes increasingly probable that the coarse references may identify wrong grid points for refined estimates in Eqs. (19) and (21). In addition, Fig. 2 also substantiates the claim that the estimates in Eqs. (15) and (16) are coarse but unambiguous. Although not shown here, the RMSEs for the second source are very similar to those in Fig. 2.

In the second example, the performance of the proposed method in terms of the SNR and the number of snapshots is respectively assessed. Specifically, we keep $\Delta = 2\lambda$ for our method and the EA algorithm, and let the SNR vary from 10 dB to 40 dB, or let the number of snapshots vary from 10 to 1000 when the SNR is fixed at 15 dB. With these simulation conditions, we compute the RMSEs of the above three algorithms, and the results for the first signal are shown in Fig. 3. It is further observed that the proposed algorithm has very similar RMSEs to those of the EA algorithm, although the latter uses more dipoles/loops (a total of 54). Fig. 3 also shows that the U-ESPRIT algorithm has significantly lower estimation precision than the other two.

In the next example, we further assess the performance of our method with $\Delta = 2\lambda$ against the SNR. Different from the above two examples, the two impinging signals are assumed to be coherent. DOA estimation using the PS-[7] and SS-based[15] ESPRIT is also performed for the performance comparisons. The SS-based ESPRIT employs an identical array with that of the above U-ESPRIT algorithm, while the PS-based ESPRIT utilizes a COLD array that contains 36 six-component electromagnetic vector-sensors constructing a $6 \times 6$ uniform rectangular geometry. Note that both of the latter algorithms require the intersensor spacing within $\Delta \leqslant \lambda/2$; we let their intersensor spacings $\Delta = \lambda/2$. The DOA RMSEs of the first coherent signal are depicted in Fig. 4. As a result of allowing the intersensor spacings to be larger than a half wavelength, the proposed algorithm can offer the refined estimates with lowest RMSEs, as shown in Fig. 4, although the PS-based ESPRIT uses an electromagnetic vector-sensor array with 6 times as many dipoles/loops as ours. In addition, due to the fact that spatial smoothing decreases the effective array aperture and the adopted array is polarization insensitive, the SS-based ESPRIT underperforms the other two methods, and its RMSEs are even greater than those of the coarse estimates of our algorithm.

It is finally worth pointing out that, in practical situations when mutual coupling effect exists, the proposed algorithm can minimize this effect by increasing the intersensor spacing, whereas the other competitors with a COLD array or USS ar-

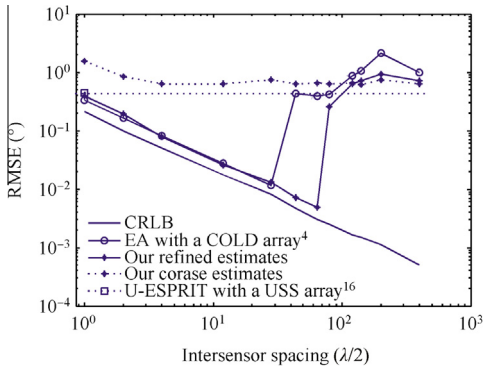


**Fig. 2** DOA RMSE vs the intersensor spacing $\Delta$.

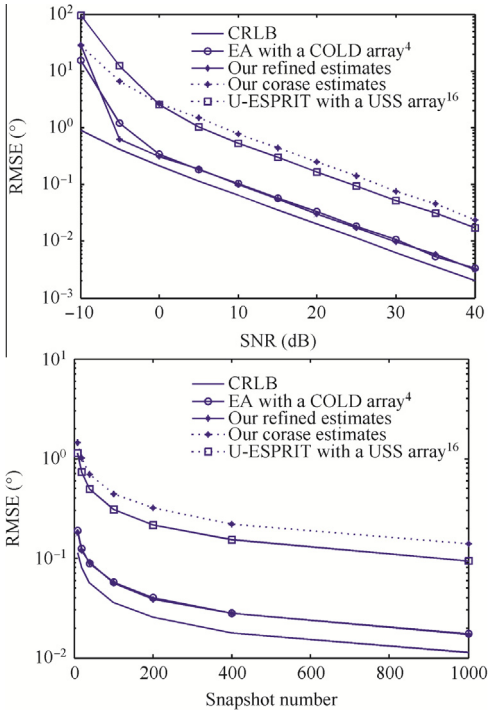


**Fig. 3** DOA RMSE vs SNR and snapshot.

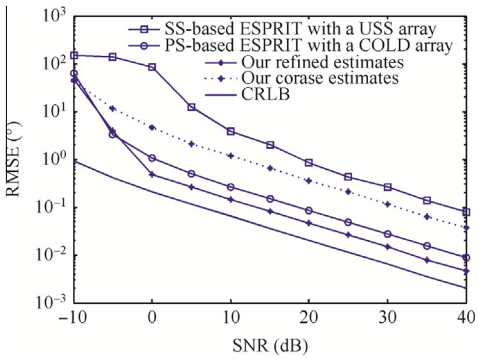


**Fig. 4** DOA RMSE vs the SNR.

ray easily suffer from this coupling effect due to the cocentered dipoles/loops or little intersensor spacing.

## 6. Conclusions

In this paper, the use of polarization information for improving source localization performance with no mutual coupling effect on array antennas is investigated, and a new localization algorithm is proposed by using a NCOLD array. Unlike the existing algorithm with the COLD arrays, the proposed algorithm allows all the dipoles/loops in the NCOLD array to be non-cocentered and well-separated, hence it demonstrates an advantage of elimination of mutual coupling and extension of the array aperture. By using the polarization information, the proposed algorithm resolves the cyclic ambiguity problem and offers high localization precision.

## Acknowledgments

This study was co-supported by the Scientific Research Fund of Zhejiang Provincial Education Department (No. Y201225848), and the Scientific and Technological Innovation Programs of Higher Education Institutions in Shanxi (No. 2013124).

## Reference

1. Wong KT, Yuan X. Vector cross-product direction-finding with an electromagnetic vector-sensor of six orthogonally oriented but spatially noncollocating dipoles/loops. *IEEE Trans Signal Process* 2011;**59**(1):160–71.
2. Wang GB, Tao HH, Wang LM. A calibration method for mutual coupling across a vector sensor. *J Electron Inf Technol* 2012;**34**(7):1558–61 [Chinese].
3. Gong XF, Liu ZW, Xu YG. Coherent source localization: bicomplex polarimetric smoothing with electromagnetic vector-sensors. *IEEE Trans Aerosp Electron Syst* 2011;**47**(3):2268–85.
4. Zoltowski MD, Wong KT. ESPRIT-based 2-D direction finding with a sparse uniform array of electromagnetic vector sensors. *IEEE Trans Signal Process* 2000;**48**(8):2195–204.
5. Zoltowski MD, Wong KT. Closed-form eigenstructure-based direction finding using arbitrary but identical subarrays on a sparse uniform Cartesian array grid. *IEEE Trans Signal Process* 2000;**48**(8):2205–10.
6. Zhang S, Guo Y, Qi Z. Joint estimation of 2D DOA and polarization with conical conformal array antenna. *J Electron Inf Technol* 2011;**33**(10):2407–12 [Chinese].
7. Rahamim D, Tabrikian J, Shavit R. Source localization using vector sensor array in a multipath environment. *IEEE Trans Signal Process* 2004;**52**(11):3096–103.
8. Liu ZT, Liu Z, He J. Polarization smoothing-based direction finding and polarization estimation of coherent sources with linear electromagnetic vector sensor array. *Acta Aeronaut Astronaut Sin* 2010;**31**(8):1646–52 [Chinese].
9. Tao J, Liu L, Lin Z. Joint DOA, range, and polarization estimation in the Fresnel region. *IEEE Trans Aerosp Electron Syst* 2011;**47**(4):2657–72.
10. Gong XF, Liu ZW, Xu YG, Ahmad MI. Direction-of-arrival estimation via twofold mode-projection. *Signal Process* 2009;**89**(5):831–42.
11. Yuan X, Wong KT, Agrawal K. Polarization estimation with a dipole–dipole pair, a dipole–loop pair, or a loop–loop pair of various orientations. *IEEE Trans Antennas Propag* 2012;**60**(5):2442–52.
12. Vorobyov SA, Gershman AB, Wong KM. Maximum likelihood direction-of-arrival estimation in unknown noise fields using sparse sensor arrays. *IEEE Trans Signal Process* 2005;**53**(1):34–43.
13. Yuan X. Coherent source direction-finding using a sparsely-distributed acoustic vector-sensor array. *IEEE Trans Aerosp Electron Syst* 2012;**48**(3):2710–5.
14. Liu Y, Wu S, Wu M, Li C, Zhang H. Wideband DOA estimation based on spatial sparseness. *Acta Aeronaut Astronaut Sin* 2012;**33**(11):2028–38 [Chinese].
15. Wang H, Liu KJR. 2-D spatial smoothing for multipath coherent signal separation. *IEEE Trans Aerosp Electron Syst* 1998;**34**(2):391–405.
16. Zoltowski MD, Haardt M, Mathews CP. Closed-form 2-D angle estimation with rectangular arrays in element space or beamspace via unitary ESPRIT. *IEEE Trans Signal Process* 1996;**44**(2):316–28.
17. Wang GM, Xin JM, Zheng NN, Sano A. Computationally efficient subspace-based method for two-dimensional direction estimation with L-shaped array. *IEEE Trans Signal Process* 2011;**59**(7):3197–212.
18. Ye Z, Zhang Y, Xu X. Two-dimensional direction of arrival estimation in the presence of uncorrelated and coherent signals. *IET Signal Process* 2009;**3**(5):416–29.
19. He J, Liu Z. Extended aperture 2-D direction finding with a two-parallel-shaped-array using propagator method. *IEEE Antennas Wireless Propag Lett* 2009;**8**:323–7.
20. Liang J, Liu D. Joint elevation and azimuth direction finding using L-shaped array. *IEEE Trans Antennas Propag* 2010;**58**(6):2136–41.

**Liu Zhaoting** received the B.S. degree in the Department of Physics from Shangrao Normal University, Shangrao, Jiangxi Province, China, in 1998, the M.S. degree in electrical engineering from Dalian Maritime University, Dalian, Liaoning Province, China, in 2005, and the Ph.D. degree in electrical engineering from Nanjing University of Science and Technology, Nanjing, Jiangsu Province, China, in 2011. Since 2005, he has been with the Shaoxing University, Shaoxing, Zhejiang Province, as a lecturer in the Electrical Engineering Department. His main research interests include radar signal analysis and processing and array signal processing.